Bathymetric Mapping of Shallow Rivers with UAV Hyperspectral Data

Valeria Gentile[1,2], Marek Mróz[3], Marie Spitoni[2], Jérôme Lejot[4], Hervé Piégay[2] and Luca Demarchi[5]
[1]*Dept. of Information, Electronics & Telecom. Eng. (DIET), Univ. of Rome "Sapienza", via Eudossiana 18, Rome, Italy*
[2]*Université de Lyon, UMR 5600 EVS, Ecole Normale Supérieure, Lyon Cedex 07, France*
[3]*Dept. of Photogrammetry & Remote Sensing, Univ. of Warmia and Mazury in Olsztyn, ul. Oczapowskiego, Olsztyn, Poland*
[4]*Université de Lyon, UMR 5600 EVS, Université Lumière Lyon 2, Campus Porte des Alpes, Bron Cedex, France*
[5]*WarsawUniversity of Life Sciences Nowoursynowska 166, 02-787 Warsaw, Poland*
valeria.gentile@uniroma1.it, {valeria.gentile, marie.spitoni, herve.piegay}@ens-lyon.fr, marek.mroz@uwm.edu.pl, jerome.lejot@univ-lyon2.fr, demarchi.luca.ld@gmail.com

Keywords: Bathymetry, High spatial resolution, Hyperspectral images, Fluvial morphology, Remote sensing.

Abstract: Airborne images have long been used to support environmental monitoring due to their synoptic capability to cover wide areas with high spatial and temporal resolution. The potential for bathymetric mapping by airborne remote sensing has been addressed and demonstrated in several studies by means of imaging and non-imaging techniques. In this paper we evaluate the potential to retrieve water depth of shallow river from high resolution hyperspectral images using an empirical model, applicable under a range of specific field conditions and in a definite interval of wavelengths.

1 INTRODUCTION

The necessity to preserve water resources and ecosystems has led to an increasing interest in monitoring the morphological status of water bodies. Through a constant data collection on the long term, it is possible to determine trends in monitored parameters and to decide suitable strategies in order to prevent river channel degradation or to restore its original status.

Remote Sensing (RS) has long been used to support environmental monitoring of fluvial environments due to its synoptic capability to cover wide areas with high spatial and temporal resolution and to detect features that are not rapidly and easily evaluable with *in situ* measurements. Remote sensing techniques have been also widely applied to assess bathymetry of water body (Carbonneau, Lane and Bergeron, 2006, Fonstad and Marcus, 2005, Lane, Westaway and Murray Hicks, 2003), being the only effective alternative to measurements collected by echo sounder mounted on boat, in very shallow and braided rivers, impossible to be entirely navigated. Furthermore ground surveys are extremely time-consuming, require a consistent deployment of manpower and provide a low spatial sampling of acquired data despite to their accuracy.

As reviewed by Feurer, Bailly, Puech, Le Coarer and Viau (2008), besides echo sounder and GPR (Ground Penetrating Radar), both requiring ground surveys, three remote sensing approaches exist for mapping water depth through imaging and non imaging techniques (Gao, 2009). These are spectral methods, photogrammetry and bathymetric LIDAR (Light Detection and Ranging). Spectral methods exploit the attenuation of electromagnetic wave through the water interface in order to derive water depth. Their capability for mapping bathymetry has been addressed in several studies, using data acquired in the visible spectrum from UAV platforms (Lejot *et al.*, 2007, Feurer *et al.*, 2008) or Airborne Thematic Mapper data simulated from ground based measurements collected through spectroradiometer (Gilvear, Hunter ad Higgings 2007) or AISA (Airborne Imaging Spectrometer for Applications) data (Legleiter, Roberts and Lawrence, 2009).

Gentile V., MrÍŇz M., Spitoni M., Lejot J., PiÃľgay H. and Demarchi L.
Bathymetric Mapping of Shallow Rivers with UAV Hyperspectral Data.
DOI: 10.5220/0006227000430049
In *Proceedings of the Fifth International Conference on Telecommunications and Remote Sensing (ICTRS 2016)*, pages 43-49
ISBN: 978-989-758-200-4

In our study we evaluate the potential to retrieve water depth of shallow river from very high resolution hyperspectral images, using a simple empirical model, applicable under a range of specific field conditions. In doing so, we take advantages first from the capability of UAV platforms to acquire very high resolution images, combined with the possibility given by hyperspectral sensors to investigate the model behaviour over a wide range of wavelengths in addition to the visible spectrum.

In our paper we provide a detailed description of the study site in section 2. In section 3 is explained the overall process to obtain the final results: the acquisition campaign with used sensors and platform is described in subsection 3.1, in subsection 3.2 the entire processing chain to derive the final orthomosaics from raw hyperspectral data cubes is illustrated, in subsection 3.3 the physical model adopted to derive the relation between the radiometric pixel value and the water depth is explained. In subsection 3.4 processing applied to the final orthomosaics to establish the goodness of the relation previously described is explained. Results and conclusion follow in sections 4 and 5 respectively.

2 STUDY SITE

The acquisition campaign was carried out along a channel reach of the Ain River in the south-east part of France. The Ain River drains a watershed surface of about 3700 km² along 200 km. It rises in the Jura Mountains, then it flows through a steep mountainous relief, before reaching its Lower Valley (Liébault and Piégay, 2002). The river in its Lower Valley flows through 50 km, in alluvial deposits (Bravard, 1986) where it is free to laterally and vertically adjust. Its depth ranges between 0 to 5 m (Lejot *et al.*, 2007). Its hydrology is dominated by snowmelt mixed with rainfall. The mean annual discharge is 120 m^3s^{-1}, ranging between 17 m^3s^{-1} to 1600 m^3s^{-1} (1-in-50 year flood) at Pont d'Ain and Chazey-sur-Ain gauging stations according to the *banque HYDRO* (http://www.hydro.eaufrance.fr/). A chain of 5 main hydroelectric dams were built until the 70's in its middle V-shape valley section. These dams have undergone important changes in the Lower Valley, *e.g.* reduction of peak flows and channel narrowing or degradation (Liébault and Piégay, 2002).

The study site (Figure 1), approximately 700 m long, between Pont d'Ain and Priay, is located in the Ain Lower Valley, northeast of the city of Lyon. It was chosen because of its fairly morphological and channel stability (paved riverbed and low lateral mobility). Due to the lack of *in situ* water depth data synchronous with imagery data, we used the simulated hydrological parameters from the numerical model developed by Paquier, Camenen, Le Coz and Béraud (2014). This model runs over ADCP and GPS cross-sectional surveys performed in 2013 and 2014 (Naudet, Le Coz, Camenen and Paquier, 2015). Riverbed changes were assumed to be negligible on the study reach since the last 3 years (the mean absolute error for the modelled 2013 water level elevation is 15 cm).

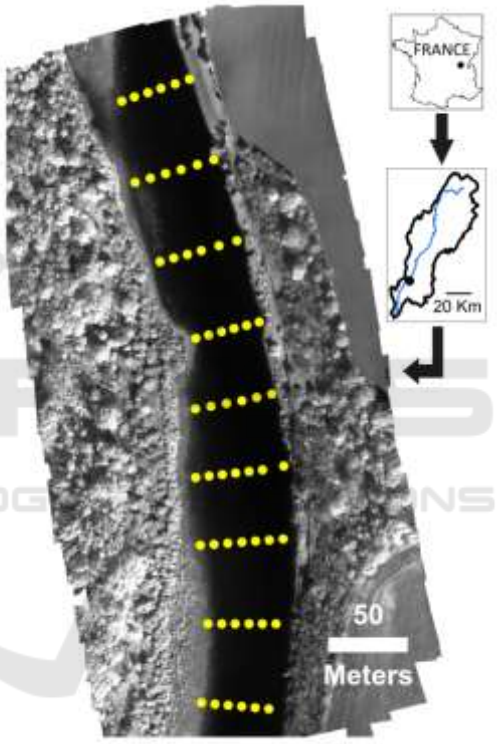

Figure 1: Orthomosaic at the central wavelength λ=776nm and geographical location of the study site; in yellow sampling points of 2D hydraulic model.

3 METHODS

3.1 Data Collection

The study area was imaged twice on 28th September 2015 in the interval 12h00-12h54 (CEST) using two coupled cameras mounted on the UAV md4-1000 quadrocopter (table 1):

- digital RGB OLYMPUS EP-2 camera

- Rikola 2D spectral sensor (Makelainen, Saari, Hippi, Sarkeala and Soukkamaki, 2013).

The Rikola 2D imaging system is a VNIR sensor based on the Piezo-Actuated Fabry-Perot Interferometer (FPI), working in the spectral range 500 nm - 900 nm. This allows the user to select the central wavelengths of the bands to be recorded by setting up the appropriate "air gaps" in the interferometer. The CCD/CMOS matrix consists of 1024x1024 detectors. Each sensing element has the size of 5.5x5.5 μm. The camera is characterized by FOV=37°, focal length f=9mm and F-number=2.8. The ADC (analog-to-digital converter) is operating in 12 bit mode. The system is equipped with GPS receiver and hemispherical irradiance sensor. The described camera model and software version permit to acquire 16 bands in full-frame mode or 24 bands in the half-frame mode (1024x648 pixels) for one "hypercube" (single frame). The user can also choose one of the two FWHMs (full width at half maximum): narrow or wide. The precise values of the FWHM for each band are determined by the interferometer itself.

Table 1: Set of spectral bands recorded in the experiment.

First flight – Full frame mode			Second flight – half frame mode		
Band no.	Central wavelength [nm]	FWHM [nm]	Band no.	Central wavelength [nm]	FWHM [nm]
1	500	15	1	500	13
2	523	20	2	516	13
3	546	19	3	532	11
4	569	18	4	548	10
5	591	18	5	564	11
6	614	19	6	580	13
7	643	13	7	596	15
8	661	19	8	612	14
9	684	17	9	628	18
10	707	18	10	644	13
11	730	18	12	676	13
12	753	17	13	692	11
13	776	18	14	708	11
14	799	17	15	724	12
15	822	19	16	740	12
16	845	18	-	-	-

The pictures were taken at the altitude MHOG=100 m (mean height over ground) forming regular blocks of strips with the end lap of 70% and side lap of 30% for hyperspectral images. The mean ground resolution of Rikola images was about 6 cm. The Rikola camera takes the hypercubes with a constant time interval Δt which was set in our experiment at 5 s.

For each block of RGB images the overlapping was bigger (80% and 40% respectively) and the ground sampling distance (GSD) was about 2 cm. The number of acquired hypercubes was bigger than 100 for each of two flights, and about 66 of RGB pictures.

3.2 Data Pre-processing

Acquired RGB images underwent orthorectification process with Agisoft Photoscan Professional software. The process consisted of digital aerotriangulation, image matching, 3D cloud point and Digital Surface Model generation and the final ortho-correction. The final RGB orthophotomap had pixel size 5x5 cm and it was considered as a background supporting the geometric processing of acquired hyperspectral data.

The exposition time for Rikola camera is usually set between 10 and 25 ms depending on sunlight intensity. In our experiment the exposition was set at 15 ms. Such a value is suitable for taking non-blurred pictures from moving platform but the technology of image formation and recording on the memory card leads to the situation where every band of the given hypercube has a slightly different position and external orientation. In these circumstances there are two alternative ways for further geometric processing:

- to adjust all bands of the hypercube to a common frame first and to produce in the next step all spectral orthomosaics in one photogrammetric run;
- to split all bands of each hypercube and to process all frames taken at the same wavelength in separated photogrammetric runs forming a set of independent spectral mosaics.

We adopted the second way because the automatic geometric adjustment/matching of the bands taken in visible and infrared spectrum is very problematic for the scenes without structural points. Therefore hyperspectral frames were processed similarly like RGB photos giving as a result a set of monochromatic orthophotomaps at the resolution of 10 cm with, unfortunately, slightly different georeferencing. The last step in geometric processing was the adjustment of all spectral orthophotomaps to the common frame by affine transformation based on RGB orthophotomap.

Prior to the orthorectification at each spectral band, the radiometric processing needed to be performed. The first step was the radiometric calibration of each hypercube to remove the influence of the black current from measured signals. The second step was the radiometric normalization *i.e.* comparison of the recorded spectral luminance for each band with the luminance of the white standardized target. In our case the Zenith Lite™ panel 50x50 cm covered by BaSO4-based white paint was used. No other atmospheric or radiometric corrections were applied. Some spectral bands from second Rikola dataset taken in half-frame mode were eliminated due to the encountered errors in pictures recording.

3.3 Bathymetric Model

The spectral radiance observed at the remote sensor detector $L_T(\lambda)$ for any wavelength λ is expressed as the sum of four components (Legleiter *et al.*, 2009):

$$L_T(\lambda) = L_B(\lambda) + L_C(\lambda) + L_S(\lambda) + L_P(\lambda) \quad (1)$$

where $L_B(\lambda)$ is the radiance reflected from bottom, $L_C(\lambda)$ is the radiance from water column, $L_S(\lambda)$ is the radiance reflected from water surface and $L_P(\lambda)$ is the path radiance from the atmosphere. Under the conditions of homogeneous water properties, shallow river, opportune viewing geometry, low acquisition altitude, favourable atmospheric conditions, highly reflective and homogeneous streambed and relatively clear water, we can consider negligible the radiance components $L_C(\lambda)$, $L_S(\lambda)$, $L_P(\lambda)$ (Legleiter et al., 2009):

$$L_T(\lambda) \approx L_B(\lambda) \quad (2)$$

where $L_B(\lambda)$ is (Philpot, 1989, Legleiter et al., 2009):

$$L_B(\lambda)=E_d(\lambda)C(\lambda)T(\lambda)(R_b(\lambda)-R_c(\lambda))\exp(-k(\lambda)d) \quad (3)$$

$E_d(\lambda)$ is the downwelling solar irradiance, $C(\lambda)$ is a constant for transmission across air water interface, $T(\lambda)$ is the transmittance of atmosphere, $R_b(\lambda)$ is the reflectance of river bottom, $R_c(\lambda)$ is the volume reflectance of water column, $k(\lambda)$ is an attenuation coefficient that accounts for absorption and scattering of light within the water column (Maritorena, Morel, Gentili, 1994, Legleiter et Al., 2009), d is the water depth. Solving with respect to water depth, we obtain:

$$\ln(L_B)=\ln(E_dCT(R_b-R_c))-kd \quad (4)$$

where we have not considered the dependence on λ to simplify the notation. The relation (4) suggests that under the above-mentioned acquisition conditions and for certain wavelengths, a relation between the remotely sensed variable L_B and the water depth can be derived and used for mapping river bathymetry. Replacing L_B with the corresponding value of digital number registered by the sensor and opportunely calibrated, after several adjustments we can rewrite (4) as a linear relation between the natural logarithm of pixel values in the image and the corresponding values of water depth:

$$d_{i,j}= a_{0,k}+a_{1,k}\ln P_{i,j,k} \quad (5)$$

where $d_{i,j}$ is the water depth in correspondence of pixel i,j in the image, $a_{0,k}$ and $a_{1,k}$ are the coefficients of linear relation related to k-th spectral band and $P_{i,j,k}$ is the value of pixel i,j at k-th spectral band.

3.4 Data Processing

Before deriving coefficients $a_{0,k}$ and $a_{1,k}$ of linear relation (5) for each orthomosaic, through a linear regression, a median filter with a window of 5x5 was applied to remove residual noise after images pre-processing.

For each spectral band, the pixel values were extrapolated from orthomosaics, in correspondence of the geographical coordinates of bathymetric values given by the numerical model of Paquier et al. (2014) applied to the Ain River (Naudet, Camenen, Le Coz, Paquier and Piégay, 2014). This 2D hydraulic model provides the riverbed elevation, the water level elevation and the water depth, based on topographic cross-sections surveyed every 50 m, increased to every 25 m where the riverbed geometry rapidly changes.

The coefficients of the linear regression of the empirical model were calculated with 70% of the samples randomly extracted from the set of samples derived in the previous step. The remaining 30% of samples were used to assess the validity of the model.

This method was repeated for each orthomosaic at each spectral band. The goodness of fitting was assessed by means of the coefficient of determination calculated on the 70% of samples and mean absolute error computed on the remaining 30% of samples.

4 RESULTS

In Figures 2, 3, 4 and 5 a subset of results from the first survey is shown. The sign of linear regression slope changes from positive to negative values, as wavelength increases. This behaviour is due to the weak correlation between water depth values and pixel values in the relation (5) at shorter wavelengths, that increases at longer wavelengths (Red and Near Infrared), when the absorption due to water column becomes stronger compared to reflectance. The increasing trend of correlation versus wavelength is more evident in Figure 6 where the coefficient of determination R^2 and the mean absolute error with respect to spectral band are shown.

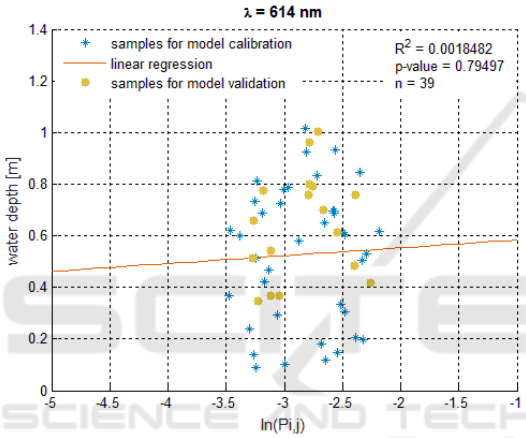

Figure 2: Linear regression at λ = 614 nm.

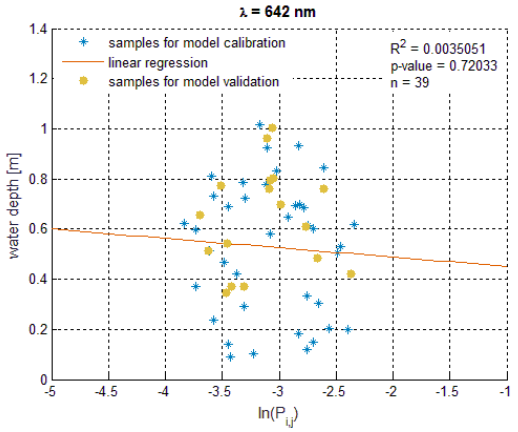

Figure 3: Linear regression at λ = 642 nm.

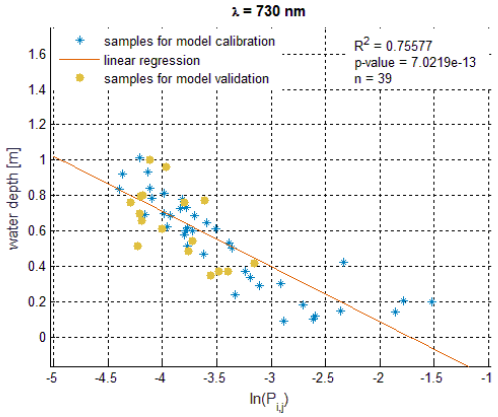

Figure 4: Linear regression at λ = 730 nm.

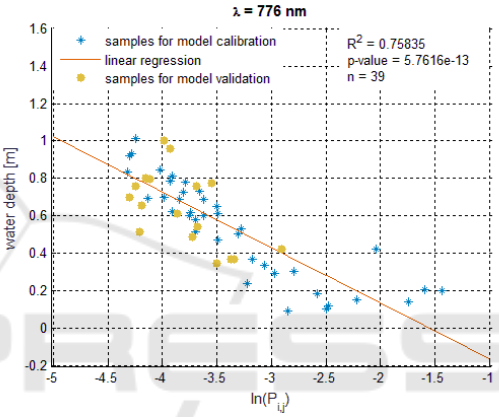

Figure 5: Linear regression at λ = 776 nm.

The best correlations are obtained in the spectral range from 700 nm to 800 nm.

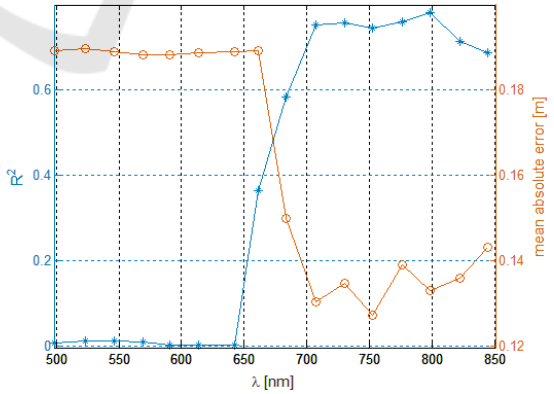

Figure 6: Trend of coefficient of determination and mean absolute error versus wavelength.

In Figures 7, 8, 9 and 10, a subset of results from the second survey is shown. In Figure 11 trends of coefficient of determination and mean absolute error with respect to spectral band are shown, confirming

both the best values of correlation in the spectral range from 700 nm to 750 nm and the increase of correlation versus wavelength, obtained in the first survey.

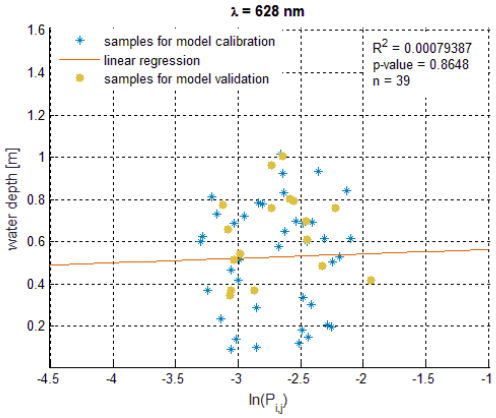

Figure 7: Linear regression at λ = 628 nm.

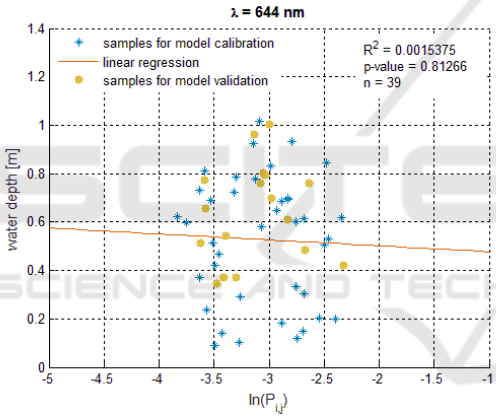

Figure 8: Linear regression at λ = 644 nm.

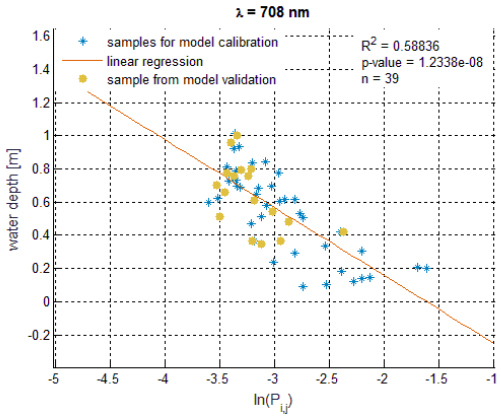

Figure 9: Linear regression at λ = 708 nm.

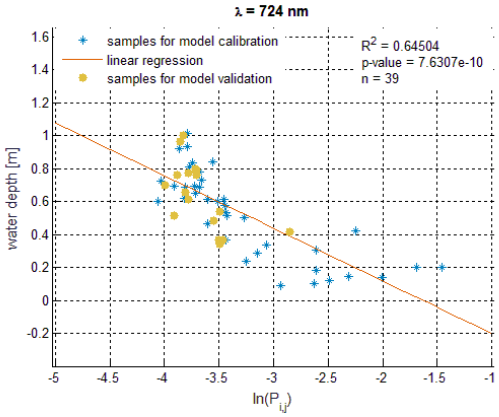

Figure 10: Linear regression at λ = 724 nm.

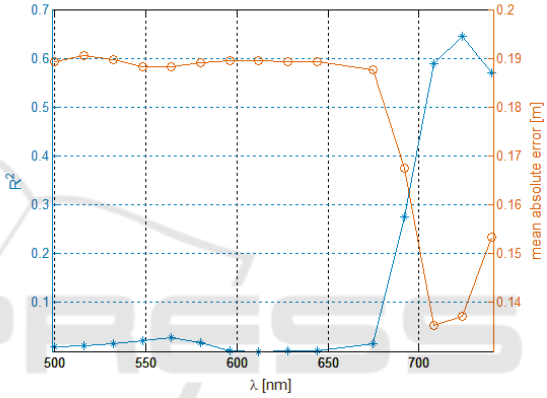

Figure 11: Trend of coefficient of determination and mean absolute error versus wavelength.

5 CONCLUSIONS

The results show the potential of UAV hyperspectral data for bathymetric mapping at centimetre resolution. The empirical model fits well the water depth values derived from the hydraulic model in the spectral range from 700 nm to 800 nm with an average error less than 0.13 m in the best case when the water depth ranges from 0.09 m to 1.01 m.

In further studies we intend to apply the proposed methodology over imagery acquired on other longer reaches of the Ain River with a wider range of water depth in order to confirm the model behaviour with respect to wavelength, to investigate its applicability over a range of wider environmental conditions, such as changes in river bottom morphology and composition, concentration in suspended sediment, water deepness and finally to examine obtained results on the basis of sensor

configuration and acquisition mode as pixel ground resolution and bandwidth.

REFERENCES

Bravard, J. P. (1986). La basse vallée de l'Ain: dynamique fluviale appliquée à l'écologie. *Recherches Interdisciplinaires sur les Ecosystémes de la Basse-Plaine de l'Ain: Potentialitees Evolutives et Gestion. Doc. Cartogr. Ecol*, *29*, 17-43.

Carbonneau, P. E., Lane, S. N., & Bergeron, N. (2006). Feature based image processing methods applied to bathymetric measurements from airborne remote sensing in fluvial environments. *Earth Surface Processes and Landforms*, *31*(11), 1413-1423.

Feurer, D., Bailly, J. S., Puech, C., Le Coarer, Y., & Viau, A. (2008). Very-high-resolution mapping of river-immersed topography by remote sensing. *Progress in Physical Geography*, *32*(4), 403-419.

Fonstad, M. A., & Marcus, W. A. (2005). Remote sensing of stream depths with hydraulically assisted bathymetry (HAB) models. *Geomorphology*, *72*(1), 320-339.

Gao, J. (2009). Bathymetric mapping by means of remote sensing: methods, accuracy and limitations. *Progress in Physical Geography*, *33*(1), 103-116.

Gilvear, D., Hunter, P., & Higgins, T. (2007). An experimental approach to the measurement of the effects of water depth and substrate on optical and near infra-red reflectance: A field-based assessment of the feasibility of mapping submerged instream habitat. *International Journal of Remote Sensing*, *28*(10), 2241-2256.

Lane, S. N., Westaway, R. M., & Murray Hicks, D. (2003). Estimation of erosion and deposition volumes in a large, gravel-bed, braided river using synoptic remote sensing. *Earth Surface Processes and Landforms*, *28*(3), 249-271.

Lejot, J., Delacourt, C., Piégay, H., Fournier, T., Trémélo, M. L., & Allemand, P. (2007). Very high spatial resolution imagery for channel bathymetry and topography from an unmanned mapping controlled platform. *Earth Surface Processes and Landforms*, *32*(11), 1705-1725.

Legleiter, C. J., Roberts, D. A., & Lawrence, R. L. (2009). Spectrally based remote sensing of river bathymetry. *Earth Surface Processes and Landforms*, *34*(8), 1039-1059.

Liébault, F., & Piégay, H. (2001). Assessment of channel changes due to long-term bedload supply decrease, Roubion River, France. *Geomorphology*, *36*(3), 167-186.

Makelainen, A., Saari, H., Hippi, I., Sarkeala, J., & Soukkamaki, J. (2013). 2D Hyperspectral frame imager camera data in photogrammetric mosaicking. *International Archives of the Photogrammetry, Remote Sensing and Spatial Information Sciences*, 263-267

Maritorena, S., Morel, A., & Gentili, B. (1994). Diffuse reflectance of oceanic shallow waters: Influence of water depth and bottom albedo. *Limnology and oceanography*, *39*(7), 1689-1703.

Naudet, G., Camenen, B., Le Coz, J., Paquier, A., & Piégay, H. (2014, June). Numerical modelling contribution to sedimentary redynamisation projects in the Ain River. In *Conférence Internationale IsRivers 2015*.

Naudet, G., Le Coz, J., Camenen, B., Paquier, A. (2015, Septembre). Modélisation numérique hydrosédimentaire 1D et 2D de la basse vallée de l'Ain. Technical report.

Paquier, A., Camenen, B., Le Coz, J., & Béraud, C. (2014). Comparison of two models for bed load sediment transport in rivers.

Philpot, W. D. (1989). Bathymetric mapping with passive multispectral imagery. *Applied optics*, *28*(8), 1569-1578.